Journal of Engineering Sciences, Assiut University, Vol. 38, No. 2, pp. 489-508, March, 2010.

INFLUENCE OF AUXILIARY EXHAUST VALVE WITH VARIABLE TIMING ON SPARK IGNITION ENGINE PERFORMANCE

Ahmed, S.A.*[*], Ibrahim, A. M.[**], Wassef, F. M.[**] and Selim, H.[**]

** : lecture assistant ** : Professor*

Mechanical Engineering Department, Faculty of Engineering, Assiut University, 71516 Assiut

(Received November 22, 2009 Accepted December 30, 2009).

New Variable valve timing strategy based on using auxiliary valve having variable timing (VVT) is used in this study. The valve is driven by a new variable valve timing mechanism constructed for this purpose. The auxiliary valve acts as an exhaust valve and the experiments and simulation model are carried out at different loads. The results show that engine performance is improved at full load and worsens at part loads. The study proves that using an auxiliary exhaust valve having variable timing is not recommended in engines applications.

NOMENCLATURE

A	Area (m^2)	x	Mass fraction, position co-ordinate
c_p, c_v	Specific heats under constant pressure, volume (J/kg.K)		**Greek Symbols**
D	Local mean diameter through intake and exhaust systems (m)	θ	Crank position angle (degree)
e	Specific internal energy (kJ/kg)	$\Delta\theta_c$	Combustion duration (degree)
f	Darcy friction factor	σ	Boltzman constant
h	Specific enthalpy (kJ/kg)	ρ	Density (kg/m^3)
k	Specific heats ratio	ϕ	Equivalence ratio
k'	Thermal conductivity (W/m.K)		**Supscripts**
m	Mass (kg)	B	Burn
N	Engine speed (rpm)	u	Unburn
Q, $\dot{q}_w$	Heat transfer (kJ), heat flux through cylinder walls (j/m^2)	w	wall
u	Local gas velocity through intake and exhaust pipes (m/s)		**Superscripts**
		$\dot{}$	Derivative with time (d/dt)
		$\bar{}$	Molar quantity

1. INTRODUCTION

Recently, variable valve timing engines (VVT) have attracted a lot of attention because of their ability to control valve events independent of crankshaft rotation, allowing for reduced pumping losses and increased brake thermal efficiency over a wider range than conventional spark-ignition engines. Variable valve timing also allows control of internal exhaust gas recirculation (by control of the valve overlap), allowing for control

of engine emissions. There are four VVT strategies [1,2,3]: (1) Phasing only the intake valve. (2) Phasing only the exhaust valve. (3) Phasing the exhaust and the intake valves equally. (4) Phasing the exhaust and the intake valves independently. In this study a new strategy is achieved by using VVT mechanism with an auxiliary valve, while both main intake and exhaust valves have fixed timing. The auxiliary valve can be used as intake or exhaust valve. In this study, it will be used as exhaust valve to study the influence of application of the new strategy on the engine performance. A new VVT mechanism, having the ability of changing valve duration and opening angle with respect to the crankshaft, is designed for controlling the auxiliary valve.

2. THEORETICAL MODEL

2.1 Assumptions

The main assumptions considered in this simulation model are: (1) Cylinder content is homogenous mixture through intake, compression, expansion and exhaust processes. (2) Two zones combustion model is assumed, each zone has a local temperature and thermodynamic properties, while pressure is uniform through the two zones. (3) Flame propagation is a spherical surface; its center is the spark plug. (4) Temperature of cylinder head, cylinder walls, piston crown, intake manifold, and exhaust manifold are constant. (5) The exhaust and intake valves are considered as converging nozzle through both forward and reverse flow. (7) Carburetor is modeled as venturi followed by an orifice representing the throttle valve.

2.2 Mathematical and Thermodynamic Submodels

Combustion Products Model For Temperature less than 1700 K, the general combustion equation for hydrocarbon fuel with air may be written as [4]:

$$C_w H_x O_y N_z \longrightarrow n_1 CO_2 + n_2 H_2O + n_3 CO + n_4 H_2 + n_5 O_2 + n_6 N_2 \tag{1}$$

Where CO moles are calculated using the water gas reaction for rich mixture.
For Temperature higher than 1700 K, eleven products are assumed [4,5]. The reaction equation is written as:

$$\begin{aligned} C_w H_x O_y N_z \longrightarrow\ & n_1 CO_2 + n_2 CO + n_3 O_2 + n_4 O + n_5 N_2 + n_6 NO \\ & + n_7 N + n_8 H_2 + n_9 H + n_{10} OH + n_{11} H_2O \end{aligned} \tag{2}$$

Where $n_1, \ldots, n_{11}$ are calculated from mass balance equations of *C, H, O* and *N* and seven dissociation reactions as given by Campbell [5] .

Thermodynamic Properties of Cylinder Content Model:

The thermodynamic properties of each species in the gas mixture inside the cylinder are calculated by using of the JANAF tables. According to this program, the thermodynamic properties of the combustion species as functions of temperature are given in polynomial form [4].

$$\bar{c}_{p_i} / \bar{R} = a_{i1} + a_{i2} T + a_{i3} T^2 + a_{i4} T^3 + a_{i5} T^4 \tag{3}$$

$$\bar{h}_i / (\bar{R}T) = a_{i1} + \frac{a_{i2}}{2}T + \frac{a_{i3}}{3}T^2 + \frac{a_{i4}}{4}T^3 + \frac{a_{i5}}{5}T^4 + \frac{a_{i6}}{T} \quad (4)$$

Values of the polynomial coefficients for each species are given in [4]. Fuel vapor thermodynamic properties are calculated by the following equations [4]:

$$\bar{c}_{Pf} = C_1 + C_2 t + C_3 t^2 + C_4 t^3 + C_5 / t^2 \quad (5)$$

$$\bar{h}_f = C_1 t + C_2 \frac{t^2}{2} + C_3 \frac{t^3}{3} + C_4 \frac{t^4}{4} - \frac{C_5}{t} + C_6 + C_7 \quad (6)$$

Where: $t=T/1000$, C_1, C_2,..., $C7$ are constants and their values are given in [4].

Engine Friction The mechanical losses due to friction between engine parts are expressed in terms of friction mean effective pressure (*fmep*). These losses are calculated according to Bishop model [6] as follows.

Piston losses:

$$(fmep)_1 = 6.2 n_r + \left\{0.606 r_c + 1.254 r_c^{1.37-0.0238 S_P}\right\} + 9.3 S_P^{1.03} \quad (7)$$

Blowby losses:

$$(fmep)_2 = 11.86 r_c^{0.4} - (3.38 + 0.103 r_c) + 6.89\left(\frac{N}{1000}\right)^{1.185} \quad (8)$$

Exhaust and inlet system throttling losses:

$$(fmep)_3 = p_{im} + p_{em} / 2.75 \quad (9)$$

Crankcase mechanical losses:

$$(fmep)_4 = 12.122\left(\frac{d\,N}{1000 l}\right) + 0.07\left\{30 - \frac{4N}{1000}\right\}\left(\frac{n_{iv} D_{iv}^{1.75}}{d^2 l}\right) + 2.688\left(\frac{N}{1000}\right)^{1.5} \quad (10)$$

Valve pumping losses:

$$(fmep)_5 = 8.96\left(\frac{N}{1000}\right)^{1.7}\left(\frac{2.98 V_d}{n_{iv} n_c D_{iv}^2}\right)^{1.298} \quad (11)$$

Cylinder Heat Transfer: Instantaneous heat transfer rate between the working fluid and the surrounding surfaces of the cylinder is calculated by using Annand equation [7].

$$q_w = \hat{a}(k'/d)(\mathrm{Re})^{\hat{b}}(T - T_w) + \hat{c}\sigma(T^4 - T_w^4) \quad (12)$$

Where: $\hat{a} = 0.5$, $\hat{b} = 0.7$, $\hat{c} = 0$ during compression and $\hat{c} = 0.4$ during the rest of cycle,

Combustion Process: Burned mass fraction of fuel is calculated by using Wiebe function [4,8]:

$$x_b = 1 - \exp\left\{-a_b\left((\theta - \theta_o)/\Delta\theta_c\right)^{b_b+1}\right\} \quad (13)$$

Where θ_o is the crank angle at which combustion starts, $\Delta\theta_c$ is the combustion duration in degrees CA, a_b=2 and b_b=5. Cylinder volume is divided into two zones, burned zone has a volume V_b and unburned zone has a volume V_u. These volumes are calculated by Annand mathematical model [9] as shown in **Fig.1**.

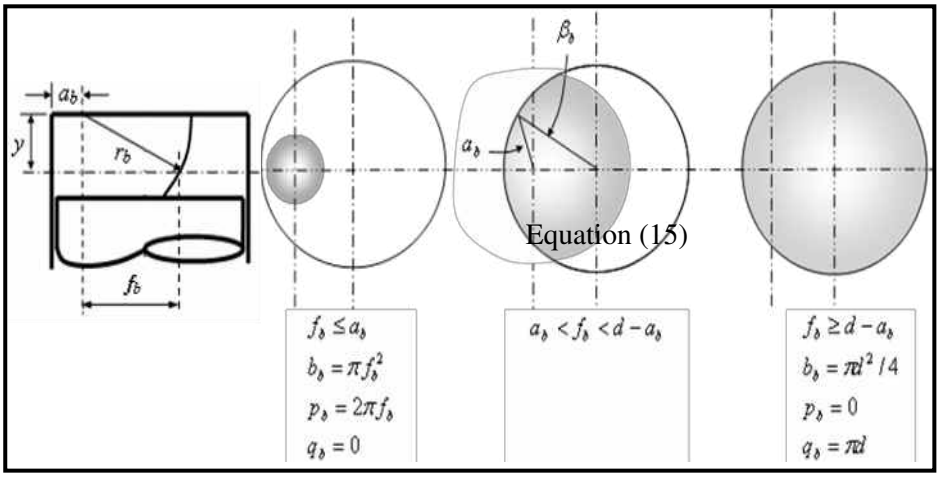

Equation (15)

Fig. 1 Flame propagation through combustion chamber

Burned volume V_b, area of flame front S_b and chamber area that is in contact with burned zone A_b are calculated by the following equations:

$$V_b = \int_0^x b_b \, dy \quad , \quad S_b = \int_0^x \left(r_b p_b / f_b\right) dy \quad \text{and} \quad A_b = \int_0^x q_b \, dy \tag{14}$$

Where f_b is the radius of intersection of flame front with plane y, p_b is the perimeter of flame front measured in plane y, and q_b is the perimeter of intersection measured in plane y.

$$\left.\begin{aligned}
&\cos\alpha = \left[\frac{a_b}{d} - \left(\frac{a_b}{d}\right)^2 - \left(\frac{f_b}{d}\right)^2\right] \Big/ \left[1 - 2a_b\left(\frac{f_b}{d}\right)\right] \\
&\cos\beta = 1 + \left[\left(\frac{a_b}{d}\right)^2 - \left(\frac{f_b}{d}\right)^2\right] \Big/ \left(0.5 - \frac{a_b}{d}\right) \\
&b_b = \left[\pi - \alpha + 0.5 \times \sin(2\alpha)\right] f_b^2 + \left[2\beta - \sin(2\beta) d^2/8\right] \\
&r_b p_b / f_b = 2(\pi - d) r \\
&q = d \times \beta
\end{aligned}\right\} \tag{15}$$

Pressure and Temperature Relationships: Applying the first law of thermodynamic for an open system on the engine cycle yields [10,11].

$$T = \frac{1}{m\, C_v}\left\{Q - pV + \sum\left(m_{in} h_{in} - m_{ex} h_{ex}\right) - em - m\sum_i e_i x_i\right\} \tag{16}$$

$$p = \frac{\rho}{\partial\rho/\partial p}\left\{\frac{m}{m} + \sum_i \frac{R_i x_i}{R} - \frac{V}{V} - \frac{\partial\rho/\partial T}{\rho} T\right\} \tag{17}$$

Where: i denotes the number of species in the working medium inside the cylinder. These equations are used in intake, compression, expansion and exhaust processes. In combustion process the cylinder is assumed to be divided into two zones, burned zone and unburned zone governed by the following equations [12,13]:

$$T_u = \frac{1}{m_u c_{pu}} \left(V_u p + Q_u \right) \tag{18}$$

$$T_b = \frac{p}{m_b R_b} \left\{ V - \left(\frac{R_b T_b}{p} - \frac{R_u T_u}{p} \right) m_b + \left(\frac{V}{p} - \frac{R_u V_u}{p\, c_{pu}} \right) p - \frac{R_u}{p\, c_{p_u}} Q_u \right\} \tag{19}$$

$$p = -\frac{1}{X^o} \left\{ \left(1 + \frac{c_{vb}}{R_b} \right) pV + \left(\left(U_b - U_u \right) - c_{vb} \left(T_b - \frac{R_u}{R_b} T_u \right) \right) m_b + Y^o Q_u - Q \right\} \tag{20}$$

Where: $X^o = Y^o V_u + \frac{c_{vb}}{R_b} V$ and $Y^o = \frac{c_{vu}}{c_{pb}} - \frac{c_{vb} R_u}{c_{p_u} R_b}$ (21)

NO_x Formation Mechanism: The extended Zeldovich mechanism mentioned in [4,8,14] is widely used. The mechanism consists of three reactions:

$$\left.\begin{aligned} O + N_2 &\longleftrightarrow NO + N \\ N + O_2 &\longleftrightarrow NO + O \\ N + OH &\longleftrightarrow NO + H \end{aligned}\right\} \tag{22}$$

These equations are solved assuming steady state formation of *N* and equilibrium values at the local pressure and temperature for *O, O_2, OH, H* and N_2. The resulting *NO* formation rate is:

$$\frac{d}{dt}[NO] = 2k_{1f}[O]_e [N_2]_e \left\{ \frac{1 - [NO]^2 / \left(K_{12} [O_2]_e [N_2]_e \right)}{1 + k_{1b} [NO] / \left(k_{2f} [O_2]_e + k_{3f} [OH]_e \right)} \right\} \tag{23}$$

Where: $K_{12} = (k_{1f}/k_{1b})/(k_{2f}/k_{2b})$, subscripts 1,2 and 3 refer to the three reactions in equation (22) of the mechanism respectively, subscript *e* refers to equilibrium, **[4]** denotes concentration in mole/cm^3. The rate constants are mentioned in [4].

CO Formation Mechanism: *CO* formation rate is calculated by the following equation which is suggested by Annand [15]:

$$\frac{d}{dt}[CO] = -10^9 \exp\left(-4500/\bar{R}T\right) \left\{ [CO][OH] - [CO_2][H] / 10^{(-1.965 + 4590/T)} \right\} \tag{24}$$

HC Emission Mechanism Unburned *HC* occurs due to flame quenching at cylinder walls, unburned mixture in cylinder craves, absorbed fuel by the oil layer and poor combustion quality. HC oxidation rate are calculated according to Lavoie model [16].

$$\frac{d}{dt}[HC] = C_R A_R [HC][O_2] \exp(-18735/T) \tag{25}$$

Where: $C_R = 2.0$ and $A_R = 6.7 * 10^{15}$ cm^3/mole.s

Flow rate Through Valves: Continuity, momentum and energy equations besides ideal gas and wave action equations are applied to the forward and reverse flow through valves [17].

Intake and Exhaust Systems: Flow through both intake, exhaust pipes and carburetor is assumed to be compressible one-dimensional, unsteady flow with friction, heat transfer and gradual area changes. The governing equations are:

1-Continuity Equation:
$$\frac{\partial \rho}{\partial t}+\rho\frac{\partial u}{\partial x}+u\frac{\partial \rho}{\partial x}+\rho\frac{u}{A}\frac{dA}{dx}=0 \tag{26}$$

2-Momentum Equation:
$$\frac{\partial u}{\partial t}+u\frac{\partial u}{\partial x}+\frac{1}{\rho}\frac{\partial p}{\partial x}+\frac{f}{D}\frac{u^2}{2}\frac{u}{|u|}=0 \tag{27}$$

3- Energy Equation:
$$\frac{\partial p}{\partial t}+u\frac{\partial p}{\partial x}-a^2\frac{\partial \rho}{\partial t}-a^2u\frac{\partial \rho}{\partial x}-(k-1)\rho\left\{q+u\frac{f}{D}\frac{u^2}{2}\frac{u}{|u|}\right\}=0 \tag{28}$$

Method of characteristics is used for solving the unsteady flow in intake and exhaust system ducts [8,19], by replacing the hyperbolic partial differential equations to total differential equations along certain characteristic lines.

Carburetor throttle valve area is simulated as an orifice. Its value is calculated according to the following equation [4]:

$$A=\frac{\pi D^2}{4}\left\{\left(1-\frac{\cos\psi}{\cos\psi_o}\right)+\frac{2}{\pi}\left[\frac{a}{\cos\psi}\left(\cos^2\psi-a^2\cos^2\psi_o\right)^{\frac{1}{2}}-\frac{\cos\psi}{\cos\psi_o}\sin^{-1}\left(\frac{a\cos\psi_o}{\cos\psi}\right)-a\left(1-a^2\right)^{\frac{1}{2}}+\sin^{-1}a\right]\right\} \tag{29}$$

Where: ψ_o, ψ are the initial and operated inclination angles of the throttle valve.

3. EXPERIMENTAL INVESTIGATION

The experimental work is carried out on a single cylinder, water cooled four stroke spark ignition engine. The engine specifications are illustrated in **table 1**. The auxiliary valve durations produced by the VVT mechanism are: 196, 204, 212, 220, 228 and 236 ^{o}CA. Experiments are carried out for five closing angles for each duration, 20 ^{o}CA BTDC, TDC, 20 ^{o}CA ATDC, 40 ^{o}CA ATDC and 50 ^{o}CA ATDC. These valve closing angles will be denoted in the following figures as -20^o, 0^o, 20^o, 40^o and 50^o CA respectively. **Figure 2** shows the VVT mechanism that controlled the auxiliary valve timing. The additional camshaft (1) leads multi-face follower (2) which moves the valve. Each face of the follower achieves valve opening duration different from the others. Additional mechanism, consists of two sliding pulleys (5) and (6), that control the valve opening angle. The valve lift profile is measured by LVDT. The LVDT is connected to an electronic circuit which is designed for magnifying its signals. The signals are displayed on a storage oscilloscope connected to PC. Both mass flow rates of air and exhaust gases through the auxiliary valve are measured by orifice meters connected to air boxes which designed according to [20] and modified according to [21,22]. Mass flow rate of fuel is calculated by determining the fuel consumed volume in 400 seconds. Brae power is measured by dynamometer.

Table 1. Engine specifications

1-	Cylinder bore ,stroke	65, 100 mm
2-	Compression ratio	6.6
3-	Start of ignition	26 deg. BTDC
4-	Main intake valve opening angle	13 deg. BTDC
5-	Main intake valve closing angle	45 deg. ABDC
6-	Main exhaust valve opening angle	45 deg. BBDC
7-	Main exhaust valve closing angle	17 deg. ATDC
8-	Intake and exhaust valves head diameter	26.5 mm
9-	Intake and exhaust valves maximum lift	5 mm
10-	Auxiliary valve maximum lift	3.2 mm
11-	Auxiliary valve head diameter	20 mm
12-	Engine speed	1200 rpm

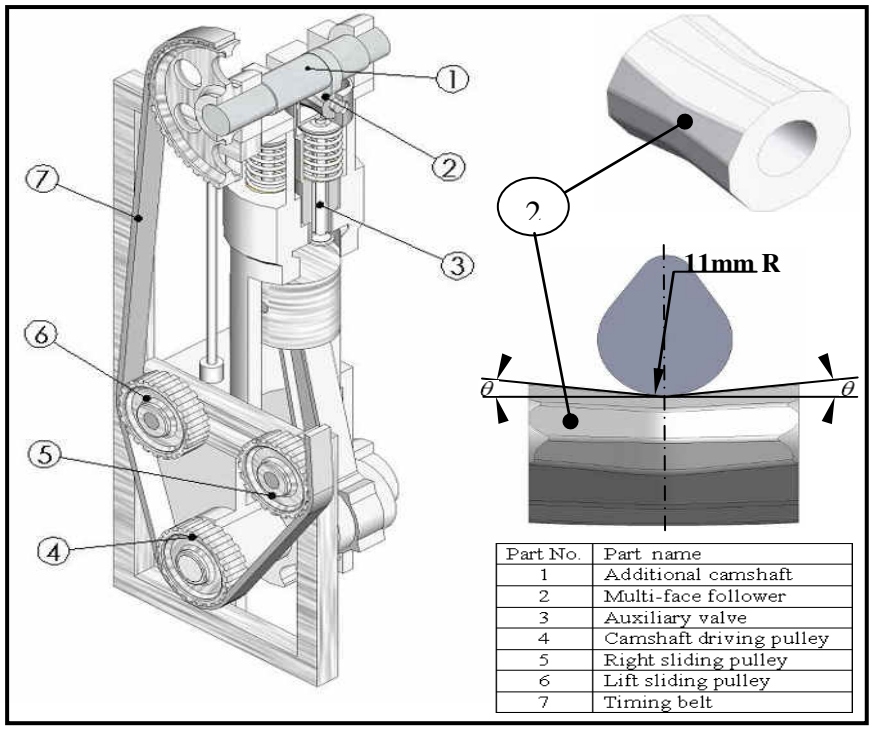

Fig. 2 The auxiliary valve and its driving mechanism assembly

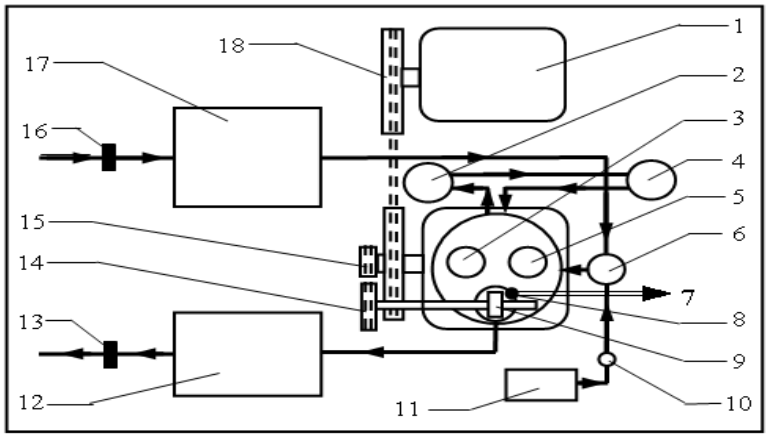

Fig. 3 Schematic diagram of the engine with the associated measuring equipments

Figure 3 shows the schematic diagram of the engine with the associated measuring equipments.

1-Dynamometer **2-** Condenser **3-** Exhaust valve **4-** Water pump **5-** Main intake valve **6-** Main carburetor **7-** LVDT terminals to electric circuit **8-** LVDT **9-** Auxiliary valve camshaft **10-** Main fuel tube **11-**Main fuel tank **12-** Exhaust surge tank **13-** Exhaust orifice meter **14-** Auxiliary camshaft driven gear **15-** Auxiliary camshaft driving gear **16-** Intake orifice meter **17-** Intake air box **18-** V-belt drive

4. VALIDATION OF THE MODEL

The validity of the present simulation model was evaluated by comparing its results with some published experimental work. **Figures 4** to **7** illustrate the agreement between experimental and simulation outputs.

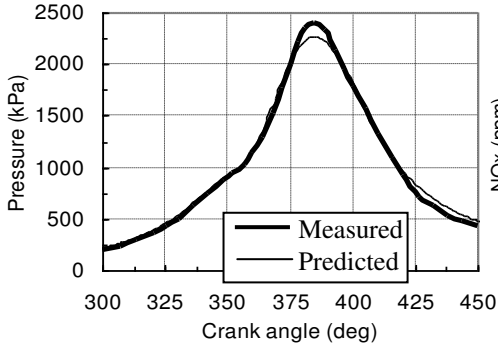

Fig. 4 Comparison between predicted and measured pressure-crank angle diagram by Ref. [23]

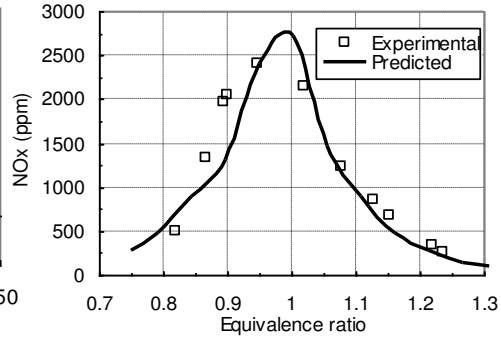

Fig. 5 Comparison between predicted and measured NO_x concentration by Ref. [24]

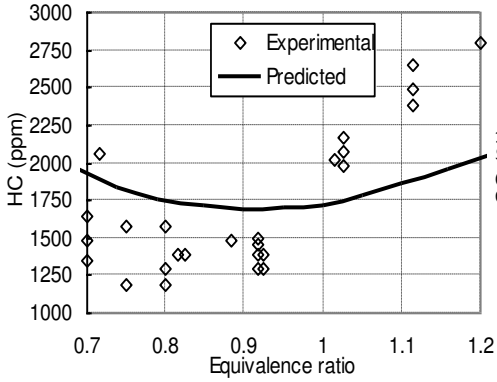

Fig. 6 Comparison between predicted and measured HC concentration by Ref. [16]

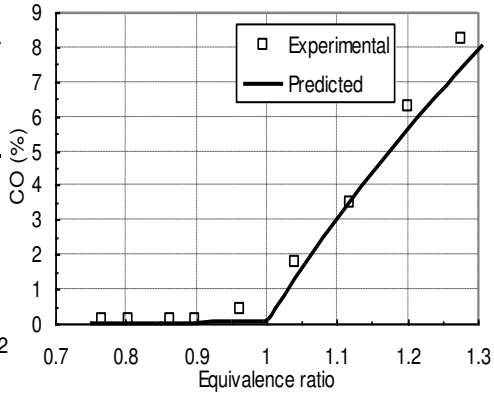

Fig. 7 Comparison between predicted and measured CO concentration by Ref. [23]

5. ORIGINAL ENGINE PERFORMANCE

We mean by "original engine" the engine without the auxiliary valve as its outputs will be taken as a reference values for comparison purpose with the VVT engine. Experiments are carried out on the engine at different loads. The loads under consideration are: **Full load (1.45 kW), 1.1 kW** (3/4 load), **0.75 kW** (1/2 load) and **0.4 kW** (1/4 load). At each load the engine parameters under consideration are: brake power, mass flow rates of air and fuel, volumetric efficiency, brake thermal efficiency and *bsfc*. The simulation model predicts residual gas fraction, CO concentration based on dry mole, NOx concentration and HC concentration. **Table 2** shows the engine performance parameters at the loads under consideration.

Table 2 Original engine performance parameters at full load and part loads

Engine parameter	Full load	1.1 kW	0.75 kW	0.4 kW
Brake thermal efficiency %	16.7	15.7	12.7	8.38
bsfc (kg/kW.h)	0.486	0.518	0.638	0.97
Mass flow rate of air (kg/s)	2.49E-3	2.15E-3	1.88E-3	1.61E-3
Mass flow rate of fuel (kg/s)	1.96E-4	1.58E-4	1.33E-4	1.08E-4
Equivalence ratio	1.19	1.11	1.07	1.01
Volumetric efficiency %	64.2	55.4	48.3	41.5
Residual gas fraction %	9.62	10.92	12.75	14.5
CO concentration %	4.86	2.95	1.88	0.61
NO_x Concentration (ppm)	207	462	646	1035
HC concentration (ppm)	2633	2591	2749	2625

6. VVT ENGINE

The experiments are carried out at full load and the same previous part loads. The same outputs are recorded for comparison. Two variation parameters are used for comparison, V_1 and V_2 as follows:

$$V_1\% = \left(\left(\xi - \xi_{orig}\right) / \xi_{org}\right) \times 100 \tag{30}$$

Where: V_1 is the variation percentage, ξ is the engine parameter under consideration and ξ_{org} is the same parameter of the original engine under the same load. As the maximum value of each engine parameter does not occur at maximum brake thermal efficiency, another variation percentage V_2 illustrates the difference between the maximum engine parameter magnitude and its value at maximum brake thermal efficiency. This variation percentage is applied for the VVT engine only. It is defined as follows:

$$V_2\% = \left(\left(\xi_{\eta_{bth\max}} - \xi_{\max}\right) / \xi_{\max}\right) \times 100 \tag{31}$$

Where: $\xi_{\max}$ s the engine parameter under consideration and $\xi_{\eta_{bth\max}}$ is the same parameter at maximum brake thermal efficiency.

6.1 Full Load

Figures 8 to **16** illustrate the engine parameters variations with both auxiliary valve opening durations and closing angles. The auxiliary valve opening durations are listed on the top of each figure.

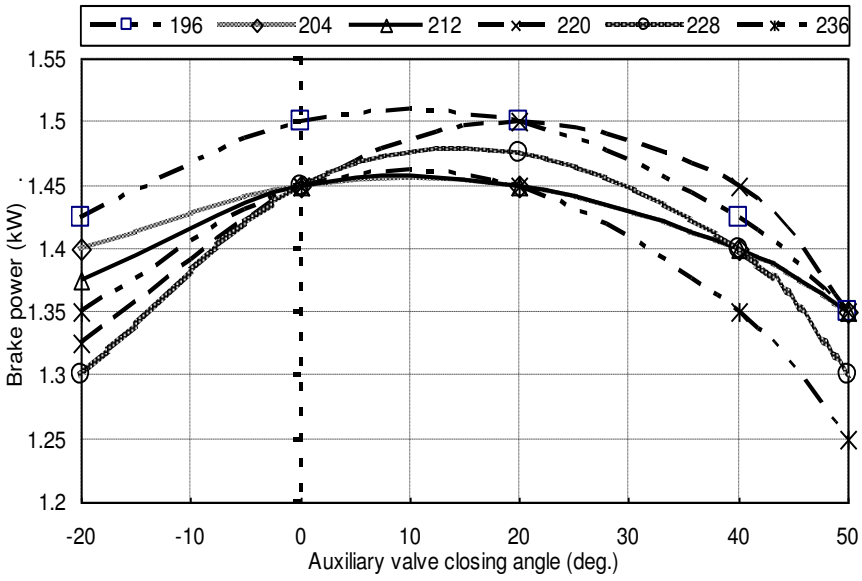

Fig. 8 Experimental variation of brake power with both auxiliary valve duration

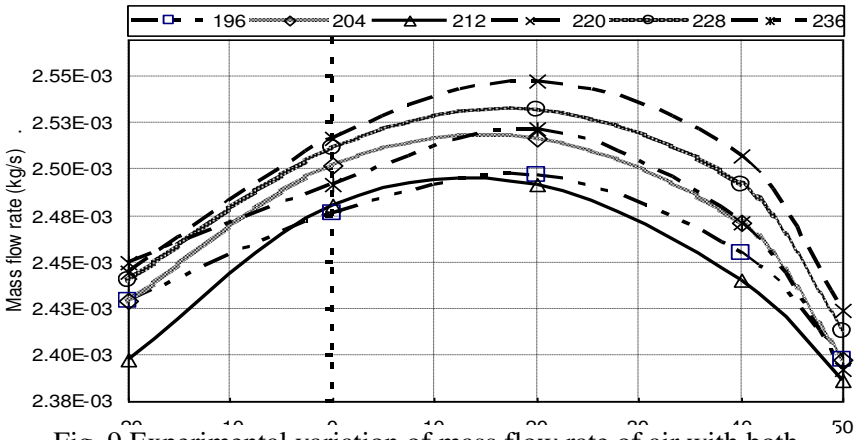

Fig. 9 Experimental variation of mass flow rate of air with both auxiliary valve duration and closing angle variations and closing angle variations

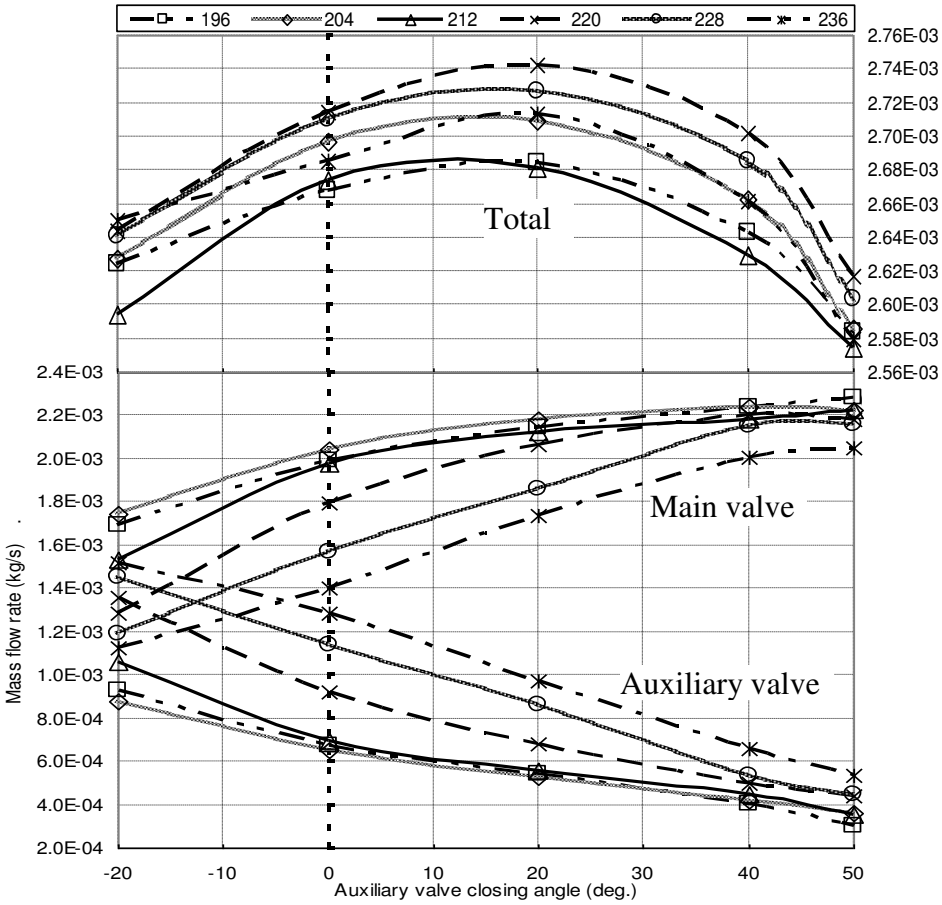

Fig. 10 Experimental variations of mass flow rates through both exhaust valves and the total mass with both auxiliary valve duration and closing angle variations

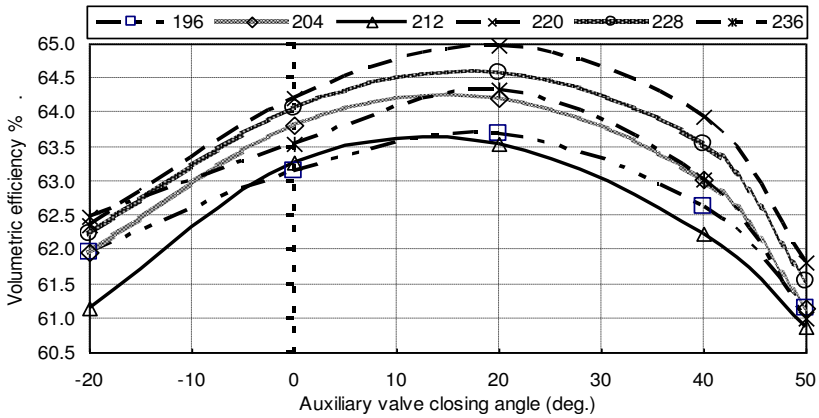

Fig. 11 Experimental variation of volumetric efficiency with both auxiliary valve duration and closing angle variations

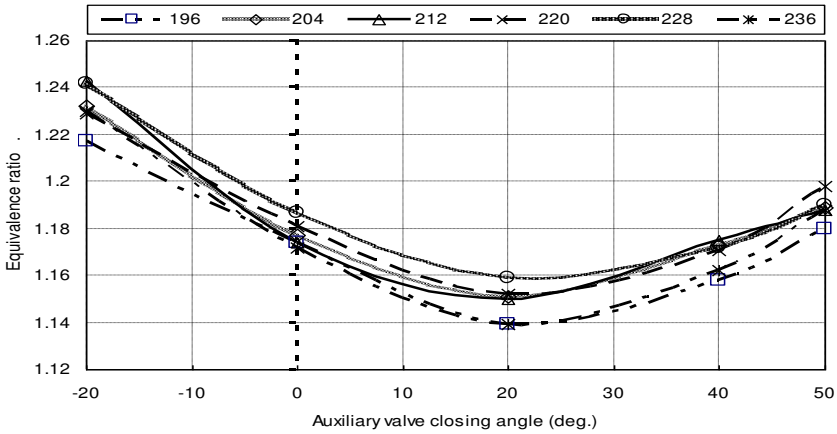

Fig. 12 Experimental variation of equivalence ratio with both auxiliary valve duration and closing angle variations

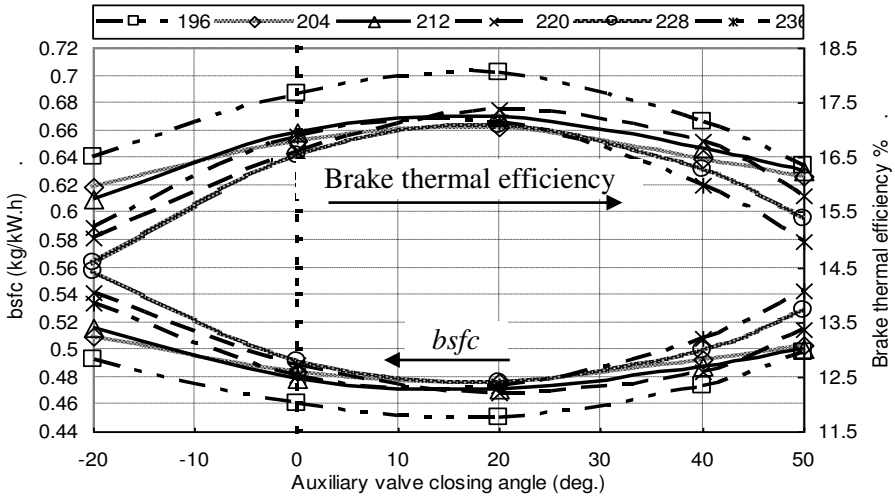

Fig. 13 Experimental variations of brake thermal efficiency and bsfc with both auxiliary valve duration and closing angle variations

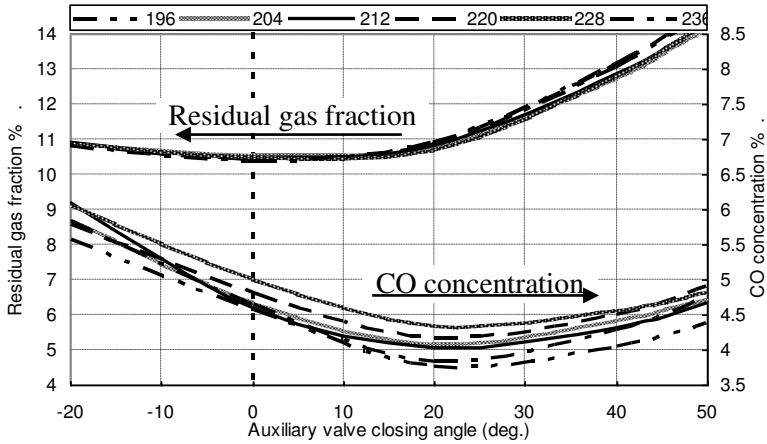

Fig. 14 Calculated variations of residual gas fraction and CO concentration with both auxiliary valve durations and closing angle variations

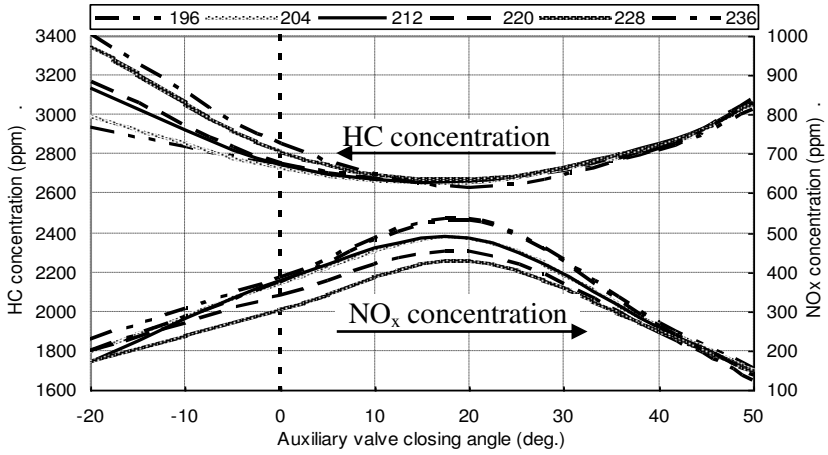

Fig. 15 Calculated variations of NO_x and HC concentrations with both auxiliary valve duration and closing angle variations

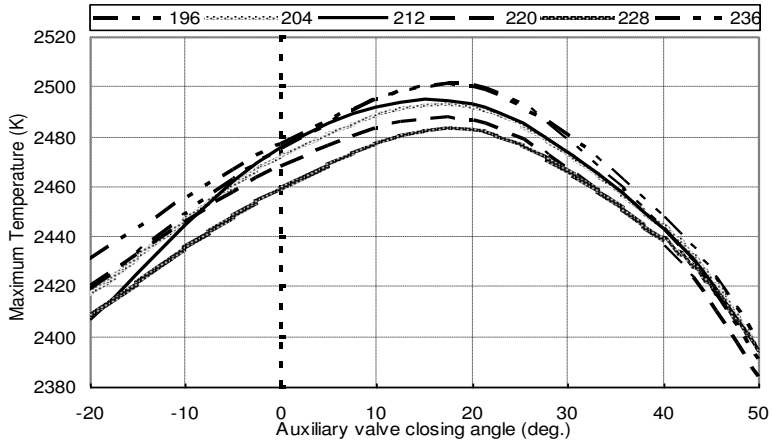

Fig. 16 Calculated variations of cylinder content maximum temperature with both auxiliary valve duration and closing angle variations

As shown in **Fig. 8**, brake power increases in the range from -20° to (10°-20°) as exhaust flow area during the valve overlap increases because of participation of auxiliary valve in it. After (10°-20°), the power decreased because of the exhaust gas reverse flow through the auxiliary valve which decreases engine charging. Maximum brake power =1.51 kW and occurs at 196° CA valve duration and 10° valve closing angle.

Mass flow rate of air through intake valve increases in the range from -20° to 20° and then decreases for the same previous reasons as shown in **Fig. 9**.

Exhaust mass flow rate through the auxiliary valve decreases while the valve closing angle moves from -20° to 50° as shown in **Fig. 10** as early opening of the valve enhances its participation in getting out the exhaust gases. For the same reason, higher valve durations have greater participation than lower valve durations.

The total mass flow rate through the exhaust valves in **Fig. 10** which represents also the fresh charge has approximately the same trend of mass flow rate of air in **Fig. 9** as the mass of fuel is relatively small compared with the mass of air.

Volumetric efficiency in **Fig. 11** has also the same trend of mass flow rate of air in **Fig. 9** for the same previous reason.

Equivalence ratio in **Fig. 12** decreases in the range of (-20 to 20) due to the increment of the mass flow rate of air in this range. Then it increases in the rest range due to the decrement of the mass flow rate of air.

Brake thermal efficiency in **Fig. 13** increases in the range from -20° to 17° then decreases following approximately the charge mass flow rate in **Fig. 10**. Maximum brake thermal efficiency happens at valve duration of 196° CA and valve closing angle of 17° with a value of 18.07% and variation percentage V_1=8.2 %. The corresponding bsfc=0.45 kg/(kW.h) with variation percentage V_1=-7.4 %. At this condition 20.8 % of the total mass of exhaust gets out through the auxiliary valve while the rest gets out through the main valve as shown in **Fig. 10**.

CO concentration in **Fig. 14** decreases in the range of -20° to 20° then increases following the trend of equivalence ratio in **Figs. 12** as the increase of equivalence ratio leads to incomplete combustion and hence CO formation increases and vice versa. Residual gas fraction in **Fig. 14** decreases in the range from -20° to 10° because of overlap improvement and then increases quickly due to the reverse flow through the auxiliary valve.

NO_x formation is an endothermal reaction depending on cylinder content temperature which increases with the increase of equivalence ratio till stoichiometric condition and then decrease at rich mixtures due to dissociation. Hence, NO_x concentration trend in **Fig. 15** follows the excess air factor which is the inverse of the equivalence ratio trend in **Fig. 12**.

HC concentration depends on the wall quench distance, craves volumes and oxidation rate. From the simulation model, it is found that, the change in wall quench distance is small as the variation in flame speed is small in the range of equivalence ratio that is achieved in these experiments and craves hydrocarbons variation is also small relative to the total amount of hydrocarbons. The important parameter is the oxidation rate which increases by cylinder content temperature increase.

Then HC in **Fig. 15** has approximately a trend opposite to the cylinder content maximum temperature in **Fig. 16**. Maximum and minimum values of the parameters

under consideration and their values at maximum brake thermal efficiency, V_1 and V_2 are illustrated in **table 3**.

From **Figs. 8** to **16** and **table 3** we can reach the following result; Valve duration of 196° CA and 17° closing angle are the best conditions for running the engine at full load as it achieve the maximum brake thermal efficiency, approximately maximum brake power and mass flow rate of fresh charge. It also achieves approximately minimum fuel consumption, residual gas fraction, CO concentration and HC concentration, in spite of achieving nearly maximum NO_x concentration.

Table 3 Magnitudes and variations of engine parameters

Engine parameter	description	magnitude	Auxiliary valve		V_1 %	V_2 %
			duration	closing angle		
Brake power (kW)	Maximum	1.51	196	10	4.1	-0.66
	At $\eta_{bth\max}$	1.5	196	17	3.75	
Mass flow rate of air (kg/s)	Maximum	2.548E-3	220	19	2.33	1.96
	At $\eta_{bth\max}$	2.498E-3	196	17	0.3	
Mass flow rate of fuel (kg/s)	Minimum	1.873E-4	196	27	-4.42	0.37
	At $\eta_{bth\max}$	1.880E-4	196	19	-4.08	
Mass flow rate of fresh charge (kg/s)	Maximum	2.742E-3	220	19	2.1	-2
	At $\eta_{bth\max}$	2.685E-3	196	17	0.05	
Equivalence ratio	Minimum	1.134	196	21	-4.65	0.26
	At $\eta_{bth\max}$	1.137	196	17	-4.45	
Volumetric efficiency %	Maximum	65	220	19	1.2	-2
	At $\eta_{bth\max}$	63.7	196	17	-0.8	
Residual gas fraction %	Minimum	9.1	228	11	-5.2	5.5
	At $\eta_{bth\max}$	9.6	196	17	-0.2	
CO %	Minimum	3.74	196	22	-23.25	1.87
	At $\eta_{bth\max}$	3.81	196	17	-21.5	
NO_x (ppm)	Maximum	540	196	18.5	160	-0.5
	At $\eta_{bth\max}$	537	196	17	159	
HC (ppm)	Minimum	2633	236	20	0.0	0.76
	At $\eta_{bth\max}$	2653	196	17	0.75	

6.2 Part loads

The same experiments and simulation are carried out at 1.1 kW, 0.75 kW and 0.4 kW. It is found that valve duration of 196° CA is the best for all loads. The suitable closing angles are 23° for 1.1 kW, 28° for 0.75 kW and 24° for 0.4 kW where the maximum

brake thermal efficiencies occurred. **Figures 17 to 24** show the different parameters variations for both original engine and VVT engine at $\xi_{\eta_{bth\max}}$ at different loads.

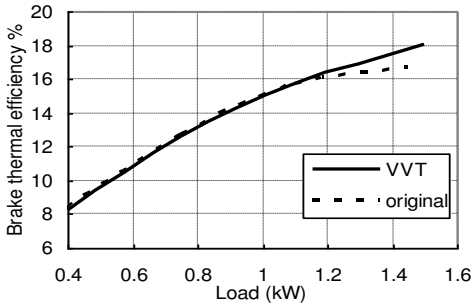

Fig.17 Variations of brake thermal efficiencies with load for original and VVT engines

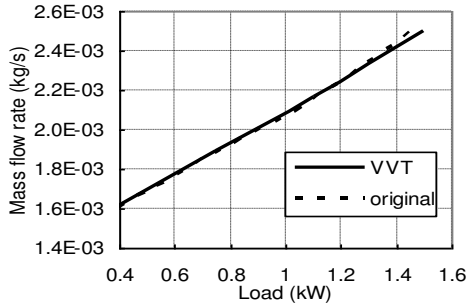

Fig.18 Variations of masses flow rate of air with load for original and VVT engines

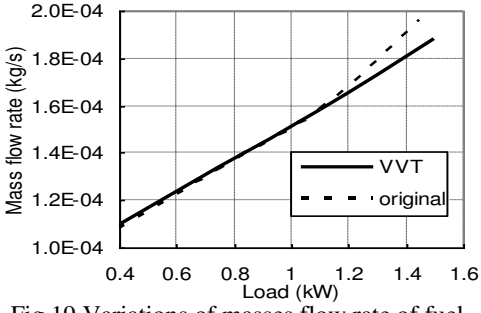

Fig.19 Variations of masses flow rate of fuel with load for original and VVT engines

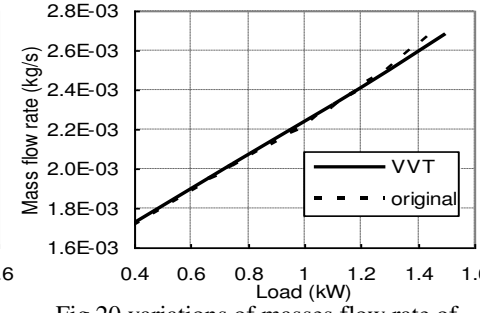

Fig.20 variations of masses flow rate of fresh charge with load for original and VVT engines

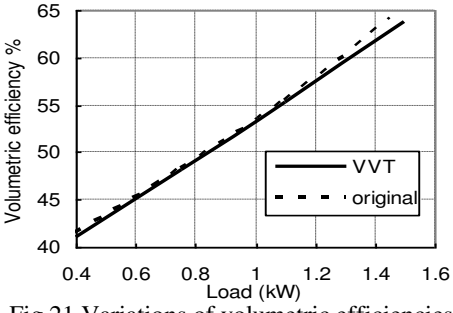

Fig.21 Variations of volumetric efficiencies with load for original and VVT engines

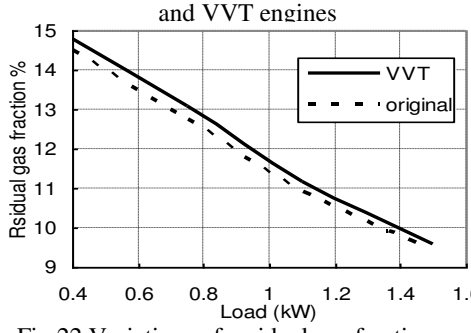

Fig.22 Variations of residual gas fractions with load for original and VVT engines

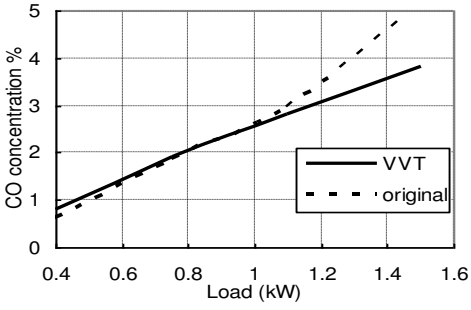

Fig.23 Variations of CO concentrations with load for original and VVT engines

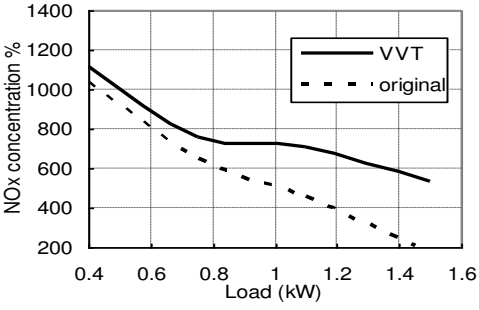

Fig.24variations of NOx concentrations with load for original and VVT engines

Table 4 shows magnitude of the same previous parameters and their variation percentages at maximum brake thermal efficiency for the different mentioned loads.

Table 4 Engine parameters at the recommended valve timing

		Full load	1.1 kW	0.75 kW	0.4 kW
Auxiliary valve	duration	196	196	196	196
	closing angle	17	23	28	24
Brake thermal efficiency	Magnitude	18.07	15.7	12.65	8.22
	Variation V_1%	8.2	0.0	-0.4	-1.9
bsfc	Magnitude	0.45	0.517	0.642	0.988
	Variation V_1%	-7.4	0.0	0.63	1.85
Mass flow rate of air (kg/s)	magnitude	2.498E-3	2.166E-3	1.888E-3	1.6125E-3
	Variation V_1%	0.32	0.74	0.43	0.12
Mass flow rate of fuel (kg/s)	magnitude	1.88E-4	1.58E-4	1.3375E-4	1.098E-4
	Variation V_1%	-4.08	0.0	0.56	1.67
Mass flow rate of fresh charge (kg/s)	magnitude	2.685E-3	2.324E-3	2.022E-3	1.722E-3
	Variation V_1%	-0.04	0.7	0.43	0.23
Auxiliary valve participation %		20.8	20.8	19.3	19.1
Volumetric efficiency %	Magnitude	63.7	55.24	48.17	41.12
	Variation V_1%	-0.8	-0.29	-0.27	-0.9
Equivalence ratio	Magnitude	1.137	1.103	1.07	1.029
	Variation V_1%	-4.45	-0.63	0.0	1.88
Residual gas fraction %	Magnitude	9.6	11.15	13.1	14.8
	Variation V_1%	-0.3	2.1	2.7	2
CO %	Magnitude	3.81	2.8	1.9	0.8
	Variation V_1%	-21.5	-5.1	1.1	12.1
NO_x (ppm)	Magnitude	537	710	760	1120
	Variation V_1%	159.5	53.6	17.6	8.2
HC (ppm)	Magnitude	2653	2760	2925	2980
	Variation V_1%	0.75	6.4	6.5	13.5

From **Figs. 17** to **24** and **table 4**, it is obvious that:

1. Brake thermal efficiency is improved at full load by 8.2 % but it decreased at part loads relative to the original engine. This means that the engine fuel consumption is increased at part loads.
2. Masses flow rates of air and fresh charge besides volumetric efficiency are mainly the same as that of the original engine at part loads.
3. Residual gas fraction increases while the load decreases and the VVT engine has a constant increase with a value of 0.3% over the whole range of load due to auxiliary valve participation in exhaust gas recirculation.
4. CO concentration decreased at small part loads and increased at moderate and full loads relative to the original engine following the same trend of the equivalences ratios of the VVT and original engines.
5. NO_x decreased over the whole range of load relative to the original engine due to the increase of residual gas fraction.
6. HC increased over the whole range of load relative to the original engine because of the decrease in oxidation rate. The oxidation rate decreases due to the decrease in cylinder content temperature which occurs due to the increase of residual gas fraction.

7. CONCLUSIONS

The present study can be summarized in the following points:

1- VVT engine performance improved at full load relative to the original engine, but it worsened at part loads.

2- VVT engine with auxiliary exhaust valve having variable timing strategy is not recommended in engine application as it cannot improve the engine performance at part loads which is the real aim in spark ignition engines.

8. REFERENCES

1. **Pierik, R. J. and Burkhard, J. F.** "Design and Development of a Mechanical Variable Valve Actuation System" SAE Technical Paper Series 2000-01-1221-March,2000.
2. **Sellnau, M.** and **Rask**, E. "Two-Step Variable Valve Actuation for Fuel Economy, Emissions, and Performance" SAE Technical Paper Series 2003-01-0029, March, 2003.
3. **Jason, M.** "Engine Modeling of an Internal Combustion Engine With Twin Independent Cam Phasing" Ph.D. Thesis, Ohio State University, 2007.
4. **Heyood, J. B."**Internal Combustion Engine Fundamentals", First Edition, McGRAW-HILL International Edition, 1988.
5. **Campbell, A.S.**" Thermodynamic Analysis of Combustion Engines ", John Willy & sons Press, 1979.
6. **Bishop, I. N."**Effect of Design Variables on Friction and Economy", SAE Transaction, Vol.3 pp 334-358, 1965.
7. **Annand, W. J. D."**Heat Transfer in Cylinders of Reciprocating Internal Combustion Engines", Proc. Instn. Mech. Engre., 177, No.36 pp 973-990, 1963.

8. **Stone, R.** "Introduction to Internal Combustion Engines" MACMILLAN PRESS LTD, 1999.
9. **Annand, W. J. D.,** "Geometry of Spherical Flame Propagation in a Disc-Shaped Combustion Chamber", Journal of Mechanical Engineering Science, Vol., 12 No., 2, 1970.
10. **Bishop, I. N."**Effect of Design Variables on Friction and Economy", SAE Transaction, Vol.3 pp 334-358, 1965.
11. **Abdel-rahim, Y. M."**Analysis and Simulation of The IC Engines Otto Cycle Using The Second Law of Thermodynamics", Ph.D. Thesis, Kansas University, U.S.A, 1984.
12. **Baghdadi, M. A.** "Computer Simulation For Combustion And Exhaust Emissions In Spark Ignition Engine Fueled With Ethanol" Department of Mechanical Engineering, The Higher Center for Engineering Comprehensive Vocations, Yefren, Libya, 2001.
13. **Bady, M. F.** "Study of the Effects of Ethanol-Gasoline Blending Ratio on the exhaust Emissions and the Performance of a Spark Ignition Engines", M. Sc. Thesis, Assiut University, 2002.
14. **Ferguson, C. R**."Internal Combustion Engines", John Willy & Sons, 1986.
15. **Annand, W. J. D.,** "A new computational Model of Combustion in Spark Ignition Engines", Proc. Instn. Mech. Engrs., Vol. 185, 1970.
16. **Lavoie, G. A.** and **Blumberg, P. N.** "Fundamental Model for Predicting Fuel Consumption, NO_x and HC Emissions of Conventional S.I.E." Combustion Science and Technology, Vol. 21, 1980.
17. **Annand, W. J. D.** and **Roa, G.E."**Gas Flow in Internal Combustion Engine", Gtfoulis and Coldt Sparkford, Yeovil Somerset, 1974.
18. **Benson, R. S. "**An Approximate Solution for Non Steady Flow in Ducts with Friction ", Ent. J. Mech. Sci., Vol. 13 pp 819-824, 1971.
19. **Azuma, T., Tokunaga, Y.** and **Yura, T."**Characteristics of Exhaust Gas Pulsation of Constant Pressure Turbocharged Diesel Engines", Journal of Engineering and Power Oct., Vol. 102/827, 1980.
20. **Kastner, L. J** "An Investigation of the Air box Method of Measuring the Air Consumption of Internal Combustion Engine" Proc. Instn. Mech. Engrs., 1953.
21. **Davies, P. O.** and **Dwger M. j."**A Simple Theory for Pressure Pulses in Exhaust Systems "Proc. Instn. Mech. Engrs., Vol. 179, No. 10, pp 365-393, 1964-65.
22. **Trengrouse, G. H.,** and **Soliman, M. M."**Effect of Sudden Change in Flow area on Pressure Wave of Finite Amplitude ", J. Mech. Eng. sci., Vol. 1948.
23. **Agarwal, A., Filib, Z. S., Assanis, D. N.** and **Barker, D. M.** "Assessment of a single and two zone turbulence formulations for quasi-dimensional modeling of spark-ignition engine combustion" Combustion Sci., and Tech., Vol., 136, 1998.
24. **Sorde, J. R.** "Modeling NO_x Emissions from Spark-Ignition Engines" Proc., Instn. Mech. Engrs. Vol 214, 2000.

تأثير وجود صمام عادم ثانوي ذو توقيت متغير على أداء محرك البنزين

تم استخدام طريقة جديدة لتغيير توقيت الصمامات تعتمد على اضافة صمام عادم ثانوي يتم التحكم فيه بميكانزم صمم خصيصا لذلك. والبحث الحالي يمثل دراسة عملية ونظرية لتطبيق هذه الطريقة مع تشغيل المحرك عند أحمال مختلفة لتحديد مدى التحسن الناتج فى أداء المحرك. تم اجراء التجارب العملية على محرك بنزين رباعي الأشواط ذو نسبة انضغاط 6.6 وسرعته 1200 لفة في الدقيقة عند: (1) الحمل الكامل . (2) 4\3 حمل. (3) 2\1 حمل. (4) 4\1 حمل. الكميات المقاسة أثناء التجارب هى معدل سريان الهواء خلال صمامى السحب الرئيسى والثانوى، معدل سريان الوقود خلال نفس الصمامين، القدرة الفرملية، القدرة الاحتكاكية. كما تم حساب نسبة الغازات المتبقية داخل الاسطوانة وانبعاثات غاز أول اكسيد الكربون وأكاسيد النيتروجين والهيدروكربون من خلال نمذج محاكي أحادي البعد. . أظهرت النتائج العملية والنظرية نسب التحسن في أداء المحرك كالتالي:

1. **الحمل الكامل:** ذادت القدرة الفرملية بمقدار 4.1 % كما ذادت الكفاءة الحرارية الفرملية بمقدار 8.2 % وقلت كتلة الشحنة الطازجة بمقدار 0.04 % كما قلت الكفاءة الحجمية بمقدار 0.8 %. وقلت كمية الغازات المتبقية بمقدار 0.21 % وأول أكسيد الكربون بمقدار 21.6 % و ذادت انبعاثات الهيدركوبون بمقدار 0.75% و انبعاثات أكاسيد النيتوجين بمقدار 159.5 %.
2. **4/3 حمل** لم تحدث أي ذيادة في الكفاءة الحرارية الفرملية بينما ذادت كتلة الشحنة الطازجة بمقدار 0.69% و قلت الكفاءة الحجمية بمقدار 0.29%. بينما ذادت كمية الغازات المتبقية بمقدار 2.1% و قلت انبعاثات أول أكسيد الكربون بمقدار 5.1% و ذادت انبعاثات الهيدركوبون بمقدار 6.5% و انبعاثات أكاسيد النيتوجين بمقدار 53.6%.
3. **2/1 حمل:** قلت الكفاءة الحرارية الفرملية بمقدار 0.4 % و ذادت كتلة الشحنة الطازجة بمقدار 0.43 % و قلت الكفاءة الحجمية بمقدار 0.27 %. و ذادت كمية الغازات المتبقية بمقدار 2.7 % وأول أكسيد الكربون بمقدار 1.1 % و ذادت انبعاثات الهيدركوبون بمقدار 6.5 % و انبعاثات أكاسيد النيتوجين بمقدار 17.6 %.
4. **4/1 حمل:** قلت الكفاءة الحرارية الفرملية بمقدار 1.9 % كما قلت كتلة الشحنة الطازجة بمقدار 0.23 % كما قلت الكفاءة الحجمية بمقدار 0.9 %. و ذادت كمية الغازات المتبقية بمقدار 2.1 % وأول أكسيد الكربون بمقدار 31.1 % و ذادت انبعاثات الهيدركوبون بمقدار 13.5 % و انبعاثات أكاسيد النيتوجين بمقدار 8.2%.

و من ذلك يتضح أن استخدام صمام عادم ثانوي ذو توقيت متغير يحسن أداء المحرك عند الحمل الكامل فقط بينما يقلل من أداء المحرك عند باقي الأحمال. لذلك لا ينصح باستخدام طريقة صمام العادم الثانوي ذو التوقيت المتغير في المحركات.